

## DISSOLUTION OF HYDROGEN SPECTRAL LINES AT HIGHER ION DENSITIES

Vladis Vujnović, Zagreb

### Abstract

In this paper\* a dissolution factor is evaluated which measures depopulation (preionization) of electron levels in strong unhomogeneous fields in a plasma. The evaluation is accomplished by constructing line profiles (in an approximate manner) for the case with dissolution and without it. The ratio of the areas under the profiles with dissolution and without dissolution, gives the dissolution factor  $W_n$  expressed by (12) and shown in Fig. 8.

### Introduction

1931 Lanczos [1] gave a wave-mechanical treatment for the decrease of hydrogen spectral line intensities in strong electric fields. The decrease in intensity even before the ionization limit is reached, is caused by stimulated ionization, preionization; owing to the broadening of terms, a discrete term-spectrum gradually transits into a continuum. Lanczos' formulae give the rate of dissolution (dissolution probability)  $\delta$  of a chosen term as a function of the field  $F$ . The energy level is depopulated and a spectral line, which is the result of the transition between the initial and final levels, shows dissolution. Now, one makes an assumption that the dissolution of the spectral line will depend practically only on the dissolution of the initial, higher level because the dissolution of lower levels is relatively much weaker. We will advocate in favour of this assumption for all members in the Lyman, Balmer and Paschen series and for higher members in the subsequent series. In an electric field, principal levels are separated into sublevels and a Stark pattern appears. Theory and experiment show that for increasing field strength, red components disappear first, dissolution proceeding towards the violet.

In calculating the dissolution of spectral lines, we follow the method of Pannekoek [2]. Pannekoek uses Lanczos' results

---

\* Communicated at XI Colloquium Spectroscopicum Internationale, Belgrade, 30. IX—4. X 1963.

studying the whole spectral-line behaviour, not the behaviour of particular line components. Inverting Lanczos' procedure, one can take a fixed rate of dissolution  $\delta$  of spectral line components and seek for the dissolved part of the total line pattern as a function of the electric field strength. The dissolved part is defined through the quantity

$$\gamma = \frac{PP''}{PP'} = \frac{\text{remaining part of Stark pattern}}{\text{total Stark pattern}},$$

(see Fig. 1). This quantity is especially useful when approximating a true, discrete Stark pattern with a rectangular area (rectangular intensity distribution inside the pattern).  $\gamma$  then means the remaining part of the total line intensity for an atom placed in a homogeneous electric field  $F$ . Also, it shows the dissolution of the  $n$ -th level because we assumed that only the initial level will govern the dissolution.

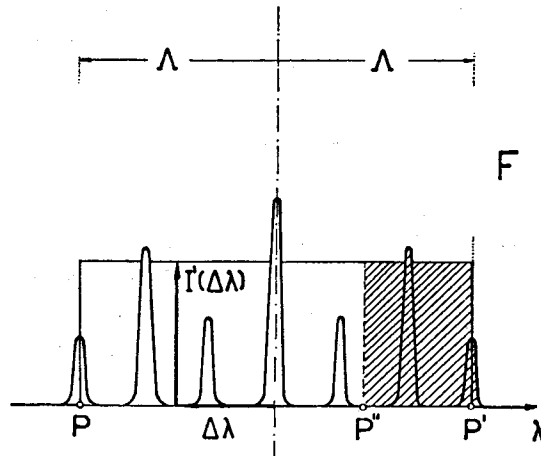


Fig. 1.

Pannekoek obtained:

$$\gamma = \frac{1,069 \times 10^6}{F n^4} - 0,259 \frac{A}{n} + 8,72 \times 10^{-9} A^2 F n^2; \quad (1)$$

$n$  is the principal quantum number of the initial level of transition and it represents the spectral line,

$F$  is the field strength in e. s. units,

$A$  is a function of  $n$ ,  $F$  and  $\delta$ :

$$A = 2,475 \times 10^6 \frac{z}{F n^3} = 9,082 - \log_{10} \delta + \log_{10} n + \log_{10} F - y, \quad (2)$$

$$z = z(y). \quad (3)$$

Details of the calculation of  $A$  and  $\gamma$  are described in Appendix I. The resulting  $A$  and  $\gamma$  are seen in Fig. 2 and 3 as functions of  $F$  with  $n$  as parameter.

The curves in Fig. 3 show the behaviour of the dissolution of Stark patterns and, consequently, of the (initial) energy levels  $n$ . The dissolution of the levels  $n = 1, 2$  and 3 starts after the dissolution of the next higher level has been completed. Considering the transitions 6—5 (or even 5—4) one cannot neglect the dissolution of the final level with regard to that of the initial level. In further procedure we use only  $n = 3$  to 6, constructing the profiles of  $H_\alpha, H_\beta, H_\gamma$  and  $H_\delta$ . To do this in an approximate manner, using the rectangular intensity distribution inside the pattern, we have to take into account intensities of all rectangles corresponding to all fields existing in a plasma.

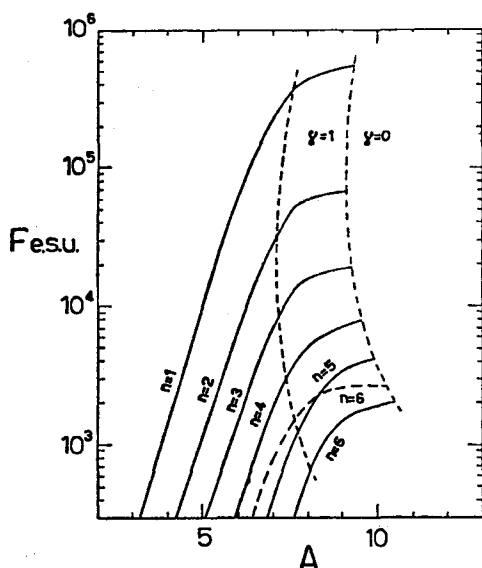


Fig. 2.

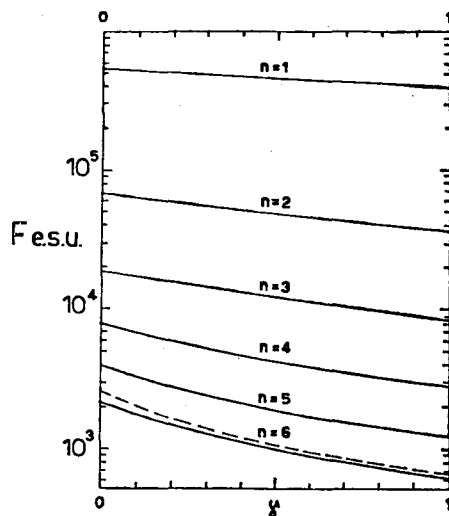


Fig. 3.

A broadened pattern of a spectral line for a given homogeneous and static field  $F$  is in the approximation represented by a rectangular area (Fig. 1). In the case of dissolution, the remaining part of the pattern is determined by the  $\gamma$ . The rectangular pattern simulates the real one. Such a pattern is approached by quasi-static ion broadening plus impact broadening of electrons: sharp spectral line components in a pattern caused by ions will be broadened and shifted by electron impacts. The field  $F$  will, therefore, have the meaning of an effective quasi-static field.

The intensity of the line in the absence of dissolution is equal to the full area of the rectangle

$$\text{Intensity } (F \text{ to } F + dF) = I'(\Delta\lambda) \cdot 2A. \quad (4)$$

In the linear Stark effect,

$$\Delta = c_n F. \quad (5)$$

An extension of the pattern depends on the applied field  $F$  and on the very nature of the pattern, expressed by  $c_n$  (the extension in a unit field). Different lines will differ in  $c_n$ .

Under conditions where there is a certain distribution of fields, line intensities will be distributed identically as to this distribution—line intensity is a result of transition in atoms, placed in fields  $F$ :

$$\text{Intensity } (F \text{ to } F + dF) = W(\beta) d\beta,$$

$$\beta \text{ is the reduced field } \frac{F_0}{F}, \quad (6)$$

$$F_0 = 2,61 e N^{2/3}.$$

$W(\beta)$  is the distribution of fields in a plasma and it depends on the charge density  $N$  and the temperature  $T$ ;  $N$  is the density of charges effective in the quasistatic manner. The number of ions or electrons to be substituted for  $N$ , will be found later by a comparison of the profiles obtained here with the exact profiles found elsewhere (the case of no dissolution).

Considering some field strength  $F$ , the spectral line intensity at a distance  $\Delta\lambda$  from the centre is equal to

$$I'(\Delta\lambda) = \frac{1}{c_n F_0} \frac{W(\beta) d\beta}{2\beta}. \quad (7)$$

To obtain the intensity at  $\Delta\lambda$ , which exists in the case of the distribution of fields, one has to sum (7) over  $\beta$ :

$$I(\Delta\lambda) = \frac{1}{c_n F_0} \int_{\beta'(\Delta\lambda)}^{\infty} \frac{W(\beta) d\beta}{2\beta} = \frac{1}{c_n F_0} U[\beta'(\Delta\lambda)], \quad (8)$$

$$\beta' = \frac{\Delta\lambda}{c_n F_0}.$$

The situation is shown in a simple way in *Fig. 4* for a definite  $F_0(N)$ . The summation of intensities at a particular distance  $\Delta\lambda$  is made over all patterns that are extended to the distance  $\Delta\lambda$ ;  $\beta'$  is a reduced field for which the end of the rectangular pattern reaches the distance  $\Delta\lambda$ . (For this pattern,  $\Delta\lambda = \Delta$ .) For stronger fields the patterns are extended further from the centre.

The area under the line profile  $I(\Delta\lambda)$  gives (by normalization) the total intensity of the line

$$I = \frac{1}{c_n F_0} \int_{-\infty}^{+\infty} U(\beta') d(\Delta\lambda) = \int_{-\infty}^{+\infty} U(\beta') d\beta' = 1. \quad (9)$$

When dissolution sets in, the shaded parts of rectangles (Fig. 4) do not exist and the intensity at a particular distance  $\Delta\lambda$  is equal to:

$$I_d(\Delta\lambda) = \frac{1}{c_n F_0} \int_{\beta'(\Delta\lambda)}^{\beta''(\gamma, \Delta\lambda)} \frac{W(\beta) d\beta}{2\beta} = \tag{10}$$

$$= \frac{1}{c_n F_0} \left\{ U[\beta'(\Delta\lambda)] - U[\beta''(\gamma, \Delta\lambda)] \right\}.$$

$\beta''(\gamma, \Delta\lambda)$  is a reduced field above which the pattern is already dissolved at the distance  $\Delta\lambda$ . For stronger fields there are no patterns with the intensity which would reach the distance  $\Delta\lambda$ .

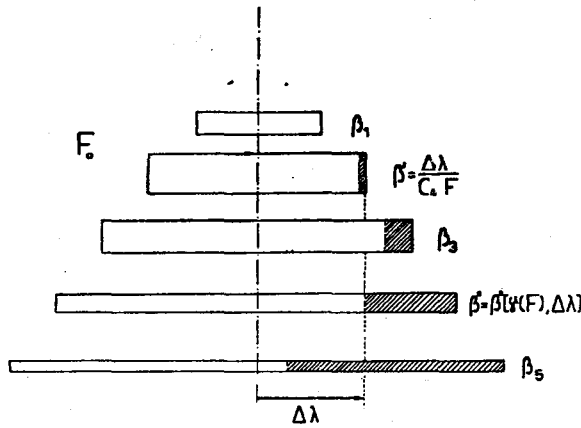


Fig. 4.

The area under the profile that suffers from dissolution is

$$I_d = \frac{1}{c_n F_0} \int_{-\infty}^{+\infty} \left\{ U[\beta'(\Delta\lambda)] - U[\beta''(\gamma, \Delta\lambda)] \right\} d(\Delta\lambda) = \tag{11}$$

$$= \int_{-\infty}^{+\infty} \left\{ U(\beta') - U[\beta''(\gamma, \beta')] \right\} d\beta'.$$

The profile construction starts by drawing the diagram shown in Fig. 5. The lines  $p$  and  $p'$ , symmetrically placed around the ordinate, indicate an extension of the profile as a function of  $F$ . For whatever  $F_0(N)$ , one can plot a separate  $\beta$ -scale on the ordinate  $F$ . From  $\beta'$  one finds  $U(\beta')$ , which is further equal to

$$U(\beta') = I(\Delta\lambda) \cdot c_n F_0.$$

In the case of dissolution, the Stark pattern will not exist for very strong fields. The »clipping« curve indicates the domain of Stark-pattern existence. It is constructed by the use of Fig. 3 and

for one spectral line it has a definite position in  $F$  vs.  $\lambda$ -plane (Fig. 5). The intensity  $I_d(\Delta\lambda)$  is obtained by a subtraction of  $U$ -values for  $\beta'$  and  $\beta''$ . The ratio of the dissolved area (11) to the not dissolved area (9) defines a dissolution factor  $W_n$ :

$$W_n = \frac{\int_{-\infty}^{+\infty} \int_{\beta'}^{\beta''} \frac{W(\beta) d\beta}{2\beta} d(\Delta\lambda)}{\int_{-\infty}^{+\infty} \int_{\beta'}^{\beta''} \frac{W(\beta) d\beta}{2\beta} d(\Delta\lambda)} = \frac{\int_{-\infty}^{+\infty} [U(\beta') - U(\beta'')] d\beta'}{\int_{-\infty}^{+\infty} U(\beta') d\beta'} = \int_{-\infty}^{+\infty} \{U(\beta') - U[\beta''(\gamma, \beta')]\} d\beta' \quad (12)$$

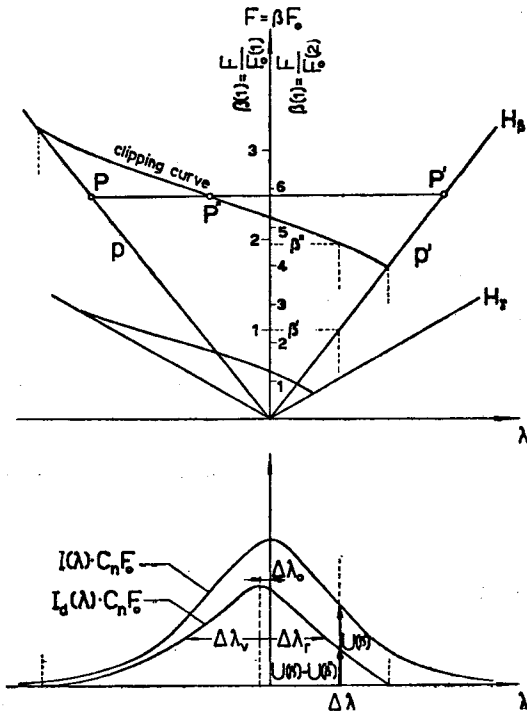


Fig. 5.

In order to obtain this factor, one should measure the total area under the dissolved profile  $I_d(\Delta\lambda)$  in the  $U(\beta')(\Delta\lambda)/c_n F_0$ -units.  $W_n$  does not depend on  $c_n$  because the shape of spectral line («relative profile») in the case of dissolution or without it does not depend on  $c_n$ . (A change in  $c_n$  causes an equal change in  $\Delta\lambda$ , and the reduced field  $\beta$ , e. g.  $\beta'$  or  $\beta''$ , will remain unchanged as an independent variable.)

**Results**

The integrals  $U(\beta')$  follow from the integration of  $W(\beta)/2\beta$  from  $\beta'$  to infinity. They depend on the distribution used. For the Holtmark distribution the integrals were found graphically by E. van Dien in 1949 [3]. We found them using the Mozer-Baranger distribution [4]. This distribution is evaluated (Tab. I on p. 628 in [4]) for low-frequency component of plasma fields which correspond to quasi-static ionic fields. In our treatment these fields should be considered as fields *effective* in the quasi-static manner.

The Mozer-Baranger distribution has a different shape for different  $N$ ,  $T$ -pairs, described by the parameter

$$\frac{r_0}{D} = 0,0898 N^{1/6} T^{-1/2}$$

( $r_0$  is the mean interionic distance,  $D$  is the Debye length). Smaller parameter means higher percentage of strong fields, or the peak of

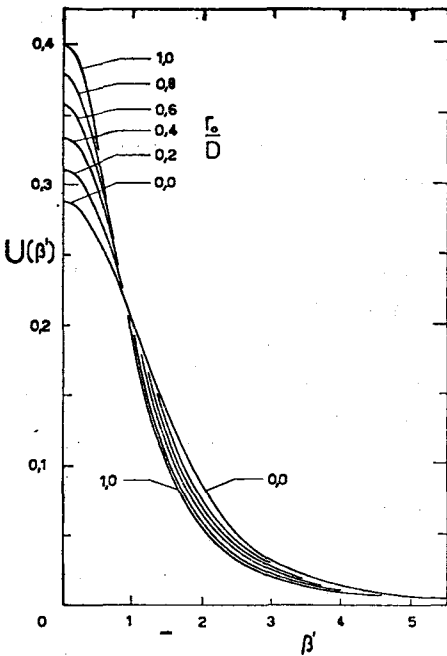


Fig. 6.

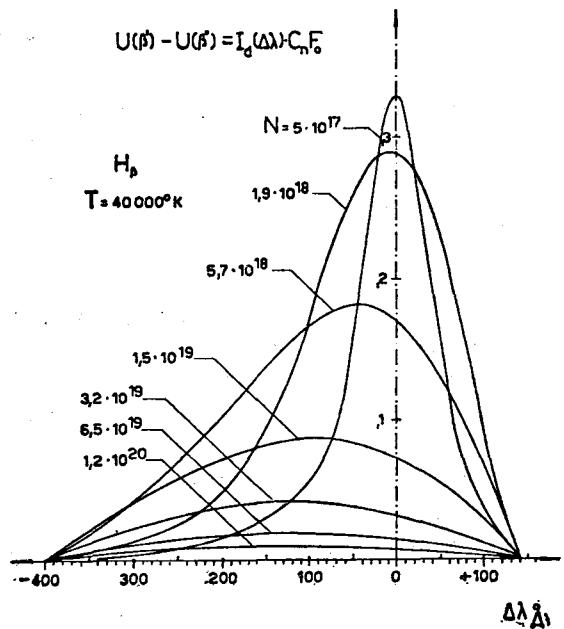


Fig. 7.

distribution is shifted towards larger  $\beta$ ; the distribution which is finally attained with  $r_0/D = 0$  is the Holtmark distribution. We evaluated the integrals  $U(\beta')$  graphically for a set of parameters  $r_0/D = 0,0$  to  $1,0$  in steps by  $0,1$ , interpolating and extrapolating the Mozer-Baranger curves. Some of our results are seen in Fig. 6. (It should be noted that parameters  $r_0/D$  larger than  $0,63$  enter into

the domain where the Debye-Hückel screening theory is not valid, which can be verified by the help of Edmonds' criterion [5].

For a fixed temperature  $T$ , the curves  $U(\beta')$  correspond to a set of  $N$ -values. Using  $T = 20.000$  and  $40.000^\circ\text{K}$ , we constructed the profiles of  $H_\alpha$ ,  $H_\beta$ ,  $H_\gamma$  and  $H_\delta$  for an interval of densities  $N$ . One example of the dissolved profiles is shown in Fig. 7. The not-dissolved profiles are of the symmetric form  $U(\beta')$ . The dissolution

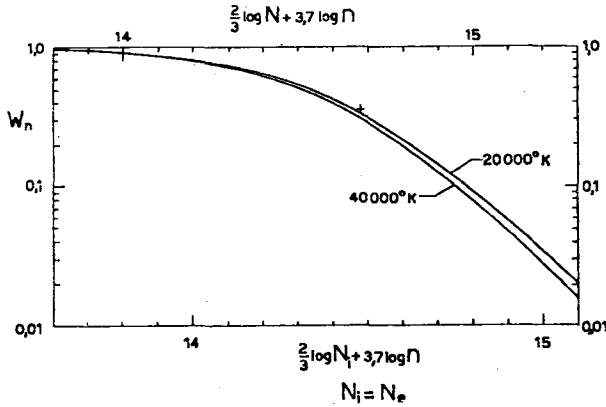


Fig. 8.

factor at the two temperatures, as function of the charge density  $N$ , was obtained by planimetry of the dissolved profiles and shown in Fig. 8. In the  $\log_{10} W_n$  vs.  $\log_{10} N$  representation, the curves for different spectral lines are nearly parallel each to other. The curves overlap with a few percent error if one plots  $\log W_n$  vs.  $\frac{2}{3} \log N + 3,7 \log n$ , the coefficient  $3,7 \pm 0,1$  found by statistical methods.

In order to demonstrate the difference in  $W_n$  due to a choice of the rate of dissolution  $\delta$ , one point was calculated for  $H_\delta$  line at  $40.000^\circ$  and  $N = 5 \times 10^{17} \text{ cm}^{-3}$  (crosses in Fig. 8 and 9) with  $\delta = A_{nm} = 9,68 \times 10^5 \text{ sec}^{-1}$  instead of  $6 \times 10^4 \text{ sec}^{-1}$ . The difference is not pronounced. One order of magnitude of difference in  $\delta$  does not affect the calculated dissolution appreciably. Also, the choice of  $\delta$  cannot explain a fairly smaller dissolution found by de Jager and Neven in 1960 [6]. A comparison with their results is made in Fig. 9.

Now we have to consider the meaning of the charge density  $N$ , effective in the quasi-static manner. We determine the value of  $N$  by comparison of our profiles with those obtained by an exact procedure of Griem, Kolb and Shen (1959, [7]). They took into account the electron impact broadening as well as the ionic field distribution based on the Debye-Hückel screening theory. Their  $N$  means  $N_{ion}$ . The absolute extension («absolute profile») measured in A. U. for instance, depends on the  $c_n$  chosen. The details of this choice are explained in Appendix II. Taking  $N = N_{ion}$

and comparing our profiles of the not-dissolved  $H_\alpha$ ,  $H_\beta$ ,  $H_\gamma$  and  $H_\delta$  (for this purpose profiles in Fig. 6 should be plotted in  $U(\beta')$  vs.

$\alpha = \frac{\Delta\lambda}{F_0} = \beta' c_n$ -scale) with the profiles in [7] we have found that our

profiles are narrower by the factor  $K = 1,6 \pm 0,1$ . The effective charge density which corresponds to the  $K$ -times wider (real) profiles should be  $K^{3/2} = 2,0 \pm 0,2$  times larger. Instead of  $N = N_{ion}$  one should take  $N = 2 N_{ion}$ . This is in accordance with the accepted fact that the broadening contribution of ions and electrons is roughly equal. The shift of the scale is seen in Fig. 8; the lower scale should be used with  $N_{ion} = N_{electron}$ .

(The use of the field distributions can be in question. We used them with  $N = N_{ion}$ . For twice larger ion density, the shape of the distribution will change. However, this change is small —  $r_0/D = 0,1$  transits to 0,11, 0,4 to 0,48, and 1,0 to 1,12 — and an iterative procedure of the profile evaluation would not be reasonable.)

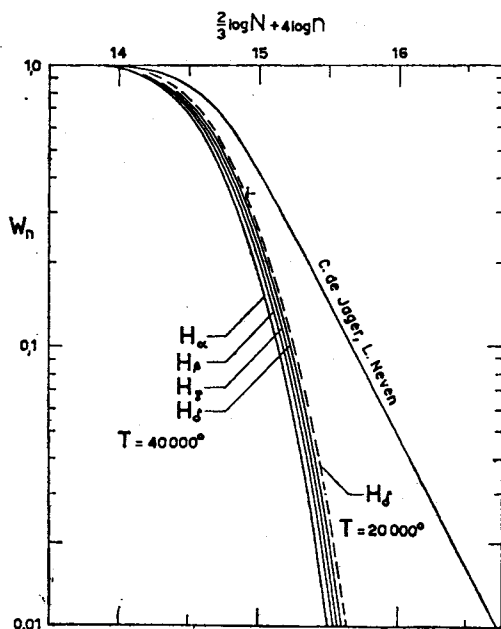


Fig. 9.

The curve for higher temperature gives stronger dissolution. This is explained by the integral (12). For higher  $T$  ( $N$  is fixed), field distributions  $W(\beta)$  have larger percentage of strong fields. Since dissolution affects more strong fields, distribution with a small parameter  $r_0/D$  will be more pronounced than the dissolution of distribution with a larger parameter. In our case, when the temperatures differ by a factor of two, the difference in dissolution is within 10% for  $W_n$  larger than 0,1 and within 10—20% for  $W_n$  between 0,1 and 0,01.

In the analysis of numerical results, we obtained a dependence on  $N^{2/3} \times n^3$ .<sup>7</sup> This has a certain physical meaning. If dissolution was caused by penetration of atoms, those orbits which are situated at the interionic mean distance will cease to exist (on the average). This distance is proportional to  $N^{-1/3}$ . If the radius of an orbit was proportional to  $n^2$  it follows that  $N^{-1/3} \times n^2$  or  $N^{2/3} n^4$  is constant for a definite dissolution. In other words,  $N^{2/3} n^4$  is variable on which the dissolution depends. Smaller power in  $n$  may have the meaning of another law for electron orbits. Under the influence of external fields, the radius of the classical orbit becomes proportional to  $n^{1.85}$ . This is equivalent to a depopulation of orbits: charge density in the electron cloud is statistically redistributed (loss of electrons in a huge number of atoms) in such a sense that the cloud looks concentrated nearer to the atomic centre.

### Conclusion

In the evaluation of the dissolution factor we used an approximate procedure which can be accomplished by graphical and numerical means. The spectral line pattern, caused by simultaneous action of ions and electrons, is represented by a rectangular area. Using this area, one should assume the quasi-static effectiveness of the corresponding fields. The effective charge density  $N$  is related to number density of ions and electrons by observing the final broadened profiles in the case of no dissolution. These profiles are very similar to the exact profiles in [7] (if one neglects details, such as a central dip in the  $H_\beta$  and  $H_\delta$ ) because sharp edges of the patterns are smoothed out due to obliteration by the field distribution. Furthermore, for an evaluation of the dissolution factor, a perfect shape of profiles is not needed because what one wants is the total area under the profiles.

This treatment was initiated owing to a lack of exact profiles in the case of high ion densities where the dissolution is noticeable. (Moreover, these exact calculation should use the field distributions which would account for the electron position in the atom. Satisfactory distributions do not exist.) The results obtained and shown in *Fig. 8* prove that the dissolution should be quite high under the conditions where individual lines are still observable and there is no Inglis-Teller merging yet. With higher fields the width of the profiles in the case of dissolution is narrower than in the case of no dissolution, the profile becomes asymmetrical with the peak shifted to the violet. In *Appendix III* we expressed the asymmetry and apparent shift of profiles as a function of  $W_n$ .

The results shown in *Fig. 8* may be used for the Lyman, Balmer, Paschen and other lines having the transition probabilities which do not differ more than by an order of magnitude from the

probabilities used in the evaluation (*Tab. I*) and having the initial and final levels not dissolved simultaneously.

The dissolution factor is needed in the evaluation of partition functions and it can serve for the purpose of eliminating a partition-function divergency. Also, the dissolution factor shows which intensity of the lines has remained in the lines or has been transferred to the continuum. This continuum stretches from the first series members towards shorter wavelengths where there is the initial series limit. The continuum represents a natural extension of the recombination continuum in the case of statistically distributed fields which cause a statistical decrease in the ionization potential.

### Appendix I

The relation (3) is given numerically in *Tab. I* of Pannekoek. For a chosen  $\delta$ ,  $n$  and  $F$ , the equations (2) and (3) give definite  $y$  and  $z$  (and  $A$ ). (It is convenient to solve the equations graphically.)

The choice of  $\delta$ , the rate of dissolution is of importance here. A spectral-line component (or generally spectral line) practically vanishes when its rate of dissolution is of the same order of magnitude as the transition probability  $A_{nm}$ . Pannekoek took  $\delta = 10^6 \text{ sec}^{-1}$  for all lines he considered near the Balmer limit; de Jager and Neven took the transition probability  $A_{n1}$  of the line in question (Lyman series). However, we suggest not to take the transition probability of the whole line but of the spectral line component:

$$A_{comp} = A_{n n_1 n_2 n_3 m m_1 m_2 m_3}$$

( $n, n_1, n_2$  and  $n_3$  are the quantum numbers in the Stark effect, the same as for  $m$ ). A choice of the total-line probability would mean that one observes the disappearance of the whole line but not of the line components. Dissolution proceeding gradually »bites off« the spectral line components and just this process is characterized by the decrease of  $\gamma$ . In the rectangular intensity approximation it is necessary to use some average of the probabilities of the spectral-line components. This average, taken over the strongest components that mainly contribute to the intensity, is shown in the following table:

Table I

Line	$H_\alpha$	$H_\beta$	$H_\gamma$	$H_\delta$	$Ly_\alpha$
$A_{nm}$	$4,39 \times 10^7$	$8,37 \times 10^6$	$2,52 \times 10^6$	$9,68 \times 10^5$	$4,68 \times 10^8 \text{ sec}^{-1}$
N <sup>o</sup> of strong components	9	10	11	16	3
Average $\delta = A_{comp}$	$5 \times 10^6$	$8 \times 10^5$	$2,3 \times 10^5$	$6 \times 10^4$	$1,6 \times 10^7 \text{ sec}^{-1}$

In this manner the evaluated coefficient  $A$  (2) as a function of the field strength  $F$  with the parameter  $n$  is plotted in Fig. 2. Curve  $n = 1$  is obtained by extrapolation of  $\delta$  and it can serve for the analysis of the dissolution of the first level. The quantity  $A$  increases with  $F$  ( $n$  is fixed) or with  $n$  ( $F$  is fixed). It is influenced by the difference in chosen  $\delta$  as shown for the case of  $n = 6$ ; the dashed curve shows the behaviour for  $\delta = A_{62} = 9,68 \times 10^5 \text{ sec}^{-1}$ .

Inserting the known values of  $A(n, F)$  into (1) we plot  $\gamma$  as a function of  $F$  with  $n$  as parameter (Fig. 3.). The dashed curve shows again the behaviour for  $\delta = 9,68 \times 10^5$ . It does not give very much difference. The reason for this is the small influence of the second and third term in  $\gamma$  (1), containing the  $A$ , on the final value of  $\gamma$ , except at higher fields. The dotted curves in Fig. 2 show the range of the coefficient  $A$  used for the evaluation of  $\gamma$  between 1,0 and 0,0.

## Appendix II

In a static and homogeneous field each component in the discrete Stark pattern has its own constant of proportionality to the applied field  $F$ . For the case of rectangular-intensity approximation, one has to apply the constant for the end of rectangle. Pannekoek used extreme spectral components for this purpose. Such a procedure is justified only when the components in the Stark pattern are equally spaced and intense, which is not the case for lower series member of hydrogen. Authors in [8] used an »equivalent rectangle width«, defined by

$$c_n = \lambda_0^2 \cdot 0,0561 \left( \sum_k I_k S_k^{3/2} \right)^{2/3} \quad (\text{c. g. s.}),$$

$\lambda_0$  is the spectral-line-centre wavelength in  $\text{cm}$ ,  $I_k$  is the relative intensity of the component ( $\sum I_k = 1$ ),  $S_k$  is the Stark coefficient (dimensionless) for the spectral line component. Using tabulated values we found:

Table II

Line	$H_\alpha$	$H_\beta$	$H_\gamma$	$H_\delta$	
$c_n$	0,0262	0,0518	0,0733	0,091	A.U./e.s.u.

## Appendix III

In order to give a rough measure of dissolution in the observed spectra, the profiles evaluated here were used to plot

$$\frac{\Delta \lambda_0}{c_n F_0} \text{ vs. } W_n, \Delta \lambda_0 \text{ in A. U., (Fig. 10)}$$

$$F_0 = 2,61 e N_i^{2/3}, N_i = N_e, \text{ and}$$

$$\frac{\Delta \lambda_v}{\Delta \lambda_r} \text{ vs. } W_n. \text{ (Fig. 11)}$$

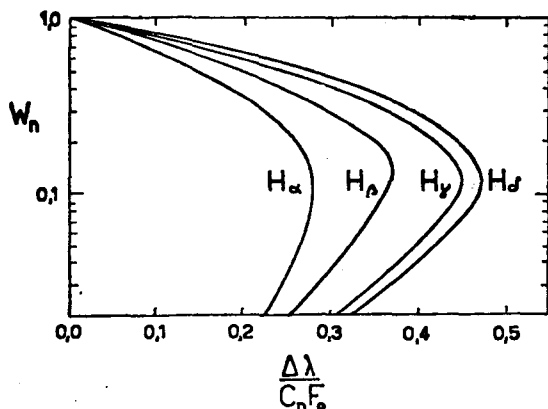


Fig. 10.

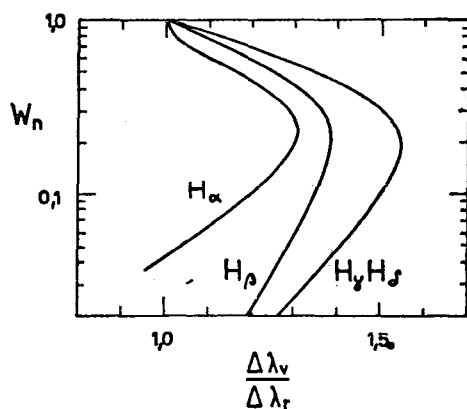


Fig. 11.

$\Delta \lambda_0$  is the apparent shift of the centre of the line towards the violet,  $\Delta \lambda_v$  and  $\Delta \lambda_r$  are the violet-side and red-side half-half widths of the profiles (see Fig. 5). The accuracy is not so high as to discriminate between different temperatures.

*Institute of Physics  
University of Zagreb*

#### REFERENCES :

- [1] C. Lanczos, Zur Intensitätsschwächung der Spektrallinien in hohen elektrischen Feldern, Z. f. Physik **68** (1931), 204,
- [2] A. Pannekoek, The hydrogen lines near the Balmer limit, M. N. **98** (1937/8), 694,
- [3] E. van Dien, The Stark effect of the higher Balmer lines in stars of spectral types A and B, Ap. J. **109** (1949), 452,
- [4] B. Mozer and M. Baranger, Electric field distributions in an ionized gas, II, Phys. Rev. **118** (1960), 626,
- [5] F. W. Edmonds, Jr., The Debye-Hückel effect and statistical theories for collisional broadening, Ap. J. **123** (1956), 95,
- [6] C. de Jager and L. Neven, The computation of partition functions in a stellar atmosphere, B.A.N. **15** (1960), 55,
- [7] H. Griem, A. Kolb and K. Y. Shen, Stark broadening of hydrogen lines in a plasma, Phys. Rev. **116** (1959), 4, and NRL Rep. № 5455 (March 1960),
- [8] C. de Jager, M. Migeotte and L. Neven, The profile of the Brackett alpha line in the solar spectrum, Ann. d'Astrophys. **19** (1956), 9.

**DISOLUCIJA SPEKTRALNIH LINIJA VODIKA KOD VELIKIH  
IONSKIH GUSTOĆA**

Vladis Vujnović, Zagreb

*Sadržaj*

U ovom radu izračunat je faktor disolucije (preionizacije) elektronskih nivoa kada su atomi smješteni u jakim, statistički raspodijeljenim poljima plazme. Za izvođenje profila spektralnih linija upotrebljena je aproksimativna metoda. Odnos površina pod profilom spektralne linije u slučaju disolucije i u slučaju kada ne bi bilo disolucije, jednak je faktoru disolucije  $W_n$  danom izrazom (12) i prikazanom u Sl. 8.

(Primljeno 11. XII 1963.)